THE JOURNAL OF BIOLOGICAL CHEMISTRY VOL. 287, NO. 7, pp. 5122–5132, February 10, 2012
Published in the U.S.A.

Solute Carrier Family 26 Member a2 (Slc26a2) Protein Functions as an Electroneutral $SO_4^{2-}/OH^-/Cl^-$ Exchanger Regulated by Extracellular Cl^-*[S]

Received for publication, August 24, 2011, and in revised form, December 14, 2011 Published, JBC Papers in Press, December 21, 2011, DOI 10.1074/jbc.M111.297192

Ehud Ohana[1,2], **Nikolay Shcheynikov**[1], **Meeyoung Park, and Shmuel Muallem**[3]

From the Epithelial Signaling and Transport Section, Molecular Physiology and Therapeutics Branch, NIDCR, National Institutes of Health, Bethesda, Maryland 20892

Background: Slc26a2 is an SO_4^{2-} transporter, mutations in which cause diastrophic dysplasia. How Slc26a2 transports SO_4^{2-} is unknown.
Results: We found that Slc26a2 exchanges SO_4^{2-} for $2OH^-$ or $2Cl^-$ and is regulated by a promiscuous extracellular anion site.
Conclusion: Slc26a2 functions as $SO_4^{2-}/2OH^-$ or $SO_4^{2-}/2Cl^-$ exchanger, regulated by extracellular Cl^-_o.
Significance: The findings should help in understanding aberrant SLC26A2 function in diastrophic dysplasia.

Slc26a2 is a ubiquitously expressed SO_4^{2-} transporter with high expression levels in cartilage and several epithelia. Mutations in SLC26A2 are associated with diastrophic dysplasia. The mechanism by which Slc26a2 transports SO_4^{2-} and the ion gradients that mediate SO_4^{2-} uptake are poorly understood. We report here that Slc26a2 functions as an $SO_4^{2-}/2OH^-$, $SO_4^{2-}/2Cl^-$, and $SO_4^{2-}/OH^-/Cl^-$ exchanger, depending on the Cl^- and OH^- gradients. At inward Cl^- and outward pH gradients (high Cl^-_o and low pH_o) Slc26a2 functions primarily as an $SO_4^{2-}{}_o/2OH^-{}_i$ exchanger. At low Cl^-_o and high pH_o Slc26a2 functions increasingly as an $SO_4^{2-}{}_o/2Cl^-{}_i$ exchanger. The reverse is observed for $SO_4^{2-}{}_i/2OH^-{}_o$ and $SO_4^{2-}{}_i/2Cl^-{}_o$ exchange. Slc26a2 also exchanges Cl^- for I^-, Br^-, and NO_3^- and Cl^-_o competes with SO_4^{2-} on the transport site. Interestingly, Slc26a2 is regulated by an extracellular anion site, required to activate $SO_4^{2-}{}_i/2OH^-{}_o$ exchange. Slc26a2 can transport oxalate in exchange for OH^- and/or Cl^- with properties similar to SO_4^{2-} transport. Modeling of the Slc26a2 transmembrane domain (TMD) structure identified a conserved extracellular sequence ^{367}GF*XX*P^{371} between TMD7 and TMD8 close to the conserved Glu^{417} in the permeation pathway. Mutation of Glu^{417} eliminated transport by Slc26a2, whereas mutation of Phe^{368} increased the affinity for $SO_4^{2-}{}_o$ 8-fold while reducing the affinity for Cl^-_o 2 fold, but without affecting regulation by Cl^-_o. These findings clarify the mechanism of net SO_4^{2-} transport and describe a novel regulation of Slc26a2 by an extracellular anion binding site and should help in further understanding aberrant SLC26A2 function in diastrophic dysplasia.

Protein sulfation, and thus SO_4^{2-}, is essential for cellular and tissue survival. Many proteins undergo post-translational modification by sulfation. Tyrosine sulfation of signaling molecules, like the G protein-coupled receptor chemokine receptors (1), modifies signaling pathways. Protein sulfation contributes to detoxification of endogenous compounds (2). A critical role of protein sulfation is sulfation of proteoglycans (3). Proteoglycans are constituents of the extracellular matrix that mediate the cell response to growth factors (4). Several disorders are caused by mutations in genes that affect proteoglycan synthesis or sulfation. The sulfate groups in proteoglycans are critical in formation of active domains, and the high polyanionic charge density of the proteoglycans is neutralized by SO_4^{2-} (5). Sulfation of secretory proteins, like digestive enzymes and mucins, is essential for their synthesis, processing through the biosynthetic pathway and packaging in secretory granules (6). Hence, understanding SO_4^{2-} homeostasis is essential for understanding cell development and function.

Cells have two sources of SO_4^{2-}, a minor source from degradation of cysteine and methionine and active uptake of SO_4^{2-} mediated largely by the SO_4^{2-} transporters Slc26a1 and Slc26a2[4] (7, 8). Slc26a1 and Slc26a2 belong to the family of the SLC26 transporters, which includes 11 genes with Slc26a10 being a pseudogene (9). Members of the family transport remarkably diverse substrates, including Cl^-, HCO_3^-, I^-, SO_4^{2-}, formant, and oxalate, and can function as coupled electroneutral or electrogenic transporters or as ion channels (9, 10). Mutations in several members of the family are associated with human diseases, including autosomal recessively inherited chondrodysplasias (SLC26A2) (11, 12), congenital chloride

* This work was supported, in whole or in part, by National Institutes of Health Grant Z1A-DE000735 from NIDCR.
[S] This article contains supplemental Figs. S1 and S2.
The amino acid sequence of this protein can be accessed through NCBI Protein Database under NCBI accession number NP_031911.
[1] Both authors contributed equally to this work.
[2] Supported by a Machiah Fellowship (Grant 2008-0702) awarded through the Machiah Foundation, a supporting foundation of the Jewish Community Federation of San Francisco, the Peninsula, Marin, and Sonoma Counties.
[3] To whom correspondence should be addressed: Epithelial Signaling and Transport Section, Molecular Physiology and Therapeutics Branch, NIDCR, National Institutes of Health, Building 10, Room 1N-113, Bethesda, MD 20892. E-mail: shmuel.muallem@nih.gov.

[4] The abbreviations used are: Slc26a1 and -a2, solute carrier family 26 isoforms a1 and a2; subscripts "*i*" and "*o*", used throughout as intracellular and extracellular, respectively; DIDS, diisothiocyanostilbene-2,2′-disulfonic acid; TMD, transmembrane domain.

diarrhea (SLC26A3) (13), Pendred syndrome (SLC26A4) (14), deafness (SLC26A5) (15), and perhaps reduced fertility (SLC26A8) (16). In addition, deletion of Slc26a6 in mice resulted in nephrolithiasis due to aberrant oxalate transport (17) and in aberrant pancreatic and parotid ducts HCO_3^- transport (18, 19).

Although Slc26a1 has limited tissue distribution, Slc26a2 is ubiquitously expressed with particularly high levels in developing and mature cartilage as well as in epithelial tissues like pancreas, salivary glands, colon, bronchial glands, tracheal epithelium, and eccrine sweat glands (20, 21). The central role of Slc26a2 in supplying the bulk of cellular SO_4^{2-} is evident from the lethality of deletion of the *SLC26A2* gene in humans and mice (20, 22), mainly due to under-sulfation of proteoglycans leading to aberrant development (23). Indeed, measurement of SO_4^{2-} uptake in fibroblast from patients with a severe form of the disease showed reduced or lack of SO_4^{2-} uptake (20, 24). Most mutations causing diastrophic dysplasia are missense mutations that affect either trafficking to the plasma membrane or showed reduced SO_4^{2-} transport (25, 26).

The phenotype of chondrodysplasias is highly variable, ranging from mild (27) to lethal before or shortly after birth (11). To better understand the disease and cellular SO_4^{2-} homeostasis, it is necessary to understand transport and regulation of Slc26a2. To date, characterization of transport by Slc26a2 was based on measurement of isotopic fluxes (24, 25, 28) that are the sum of both net and exchange fluxes, with the exchange dominating the fluxes. These studies revealed that Slc26a2 can transport SO_4^{2-}, Cl^-, and oxalate (24, 25, 28), and a recent detailed characterization of the fluxes suggested that Slc26a2 functions as an electroneutral transporter when mediating isotopic fluxes. SO_4^{2-} fluxes appeared to be sensitive to intracellular and extracellular pH (24). An unusual finding was that inhibition of SO_4^{2-} and oxalate isotopic uptake by external Cl^- exhibited simple saturation, whereas Slc26a2-mediated exchange of intracellular SO_4^{2-}, oxalate, or Cl^- for external Cl^- was non-saturable (24), suggesting that the measured fluxes, at least isotopic efflux, is mostly exchange rather than net fluxes.

The available information is not sufficient to determine the mode of SO_4^{2-} and other ions transport by Slc26a2 and the cellular ionic gradients that drive net transport. We used *Xenopus* oocytes expressing Slc26a2 to report that Slc26a2 functions as $SO_4^{2-}/2OH^-$, $SO_4^{2-}/2Cl^-$, and $SO_4^{2-}/OH^-/Cl^-$ exchanger, depending on the cellular Cl^- and $OH^-(H^+)$ gradients. Slc26a2 can also mediate $Ox^{2-}{}_o/OH^-{}_i/Cl^-{}_i$ exchange and transport I^-, Br^-, and NO_3^-. Slc26a2 activity is regulated by an extracellular anion binding site, which is not involved in ion transport. Modeling of the Slc26a2 transmembrane sector identified an extracellular loop, which contains the conserved sequence ^{367}GF*XX*P^{371} in the vicinity of the gating Glu^{417} as a potential part of the permeation pathway. These findings should help in further understanding ion transport by the SLC26 transporters and aberrant SLC26A2 function in diastrophic dysplasia.

EXPERIMENTAL PROCEDURES

Solutions and Reagents—For experiments in oocytes, the standard HEPES-buffered ND96 solution contained (in mM): 96 NaCl, 2 KCl, 1.8 $CaCl_2$, 1 $MgCl_2$, and 5 HEPES, pH 7.5. Cl^--free solutions were prepared by replacing chloride with gluconate in the presence of calcium cyclamate substituted for $CaCl_2$. A 100 mM solution of diisothiocyanostilbene-2,2′-disulfonic acid (DIDS) (Invitrogen) dissolved in DMSO was prepared freshly and diluted to a final concentrations of 10 or 50 μM in the relevant solutions. All other chemicals and reagents were purchased from Sigma.

cRNA Preparation—The pCMV-Sport6-Slc26a2 (GenBank™/EMBL/DDBJ, accession no. BC028345) was purchased from Open Biosystems and was used as template for cRNA preparation. The plasmid was linearized with NotI and used to transcribe cRNA with an mMESSAGE mMACHINE Sp6 kit (Life Technologies, Applied Biosystems), respectively. Mutation in Slc26a2 were generated by a site-directed mutagenesis kit (Agilent Technologies) and verified by sequencing.

Biotinylation and Western Blot Analysis—To monitor surface expression of Slc26a2 WT, E417A, and E417K, HEK cells transfected with vector alone or Myc-tagged Slc26a2 constructs were incubated with EZ link Sulfo-NHS-LC-Biotin (0.5 mg/ml, Thermo Fisher Scientific) for 30 min at room temperature. Subsequent steps were as previously described (29) with the following modifications: 50 μl of 1:1 slurry of immobilized avidin beads (Thermo Fisher Scientific) was added to 300 μg of protein in 300 μl of cell extract, and the mixture was incubated overnight. To monitor protein expression the PVDF membranes were incubated overnight with anti-Myc antibodies diluted 1:1,000 (Cell Signaling) and for 1 h with HRP-conjugated goat anti-mouse (Invitrogen) diluted 1:2,000. For β-actin detection membranes were incubated for 1 h with monoclonal anti-β-actin peroxidase (Sigma-Aldrich) diluted 1:20,000.

Xenopus laevis Oocyte Preparation—All experiments in this study were conducted under the National Institutes of Health guidelines for research on animals, and experimental protocols were approved by the Institutional Animal Care and Use Committee. Oocytes were isolated by partial ovariectomy of anesthetized female *X. laevis* (*Xenopus* Express, Brooksville, FL) and treated by collagenase B (Roche Applied Science), as described previously (30). Stage V–VI oocytes were injected with 10 ng of cRNA using glass micropipettes and a microinjection device (Nanoliter 2000; World Precision Instruments) in a final volume of 27.6 nl. Control oocytes were injected with equal volumes of H_2O. Oocytes were incubated at 18 °C in ND96 supplemented with 2.5 mM pyruvate and antibiotics and were studied 72–144 h after injection.

Voltage, pH, and Cl^- Measurement in Oocytes—Voltage recordings were performed at room temperature with two-electrode voltage clamp, exactly as described previously (29, 30). Voltage, pH_i, and $Cl^-{}_i$ concentrations were measured as detailed previously (31, 32). In the present study, the Cl^--sensitive electrode was also used to record intracellular Br^-, I^-, and NO_3^- with the resin and the procedure used to measure Cl^- (see "Results").

Measurement of Buffer Capacity—To determine $OH^-(H^+)$ fluxes by Slc26a2 we determined the buffer capacity of oocytes bathed in HEPES-buffered medium. Because we can measure both $Cl^-{}_i$ and pH_i, we determined the buffer capacity directly rather than relying on pH_i changes induced by weak acids.

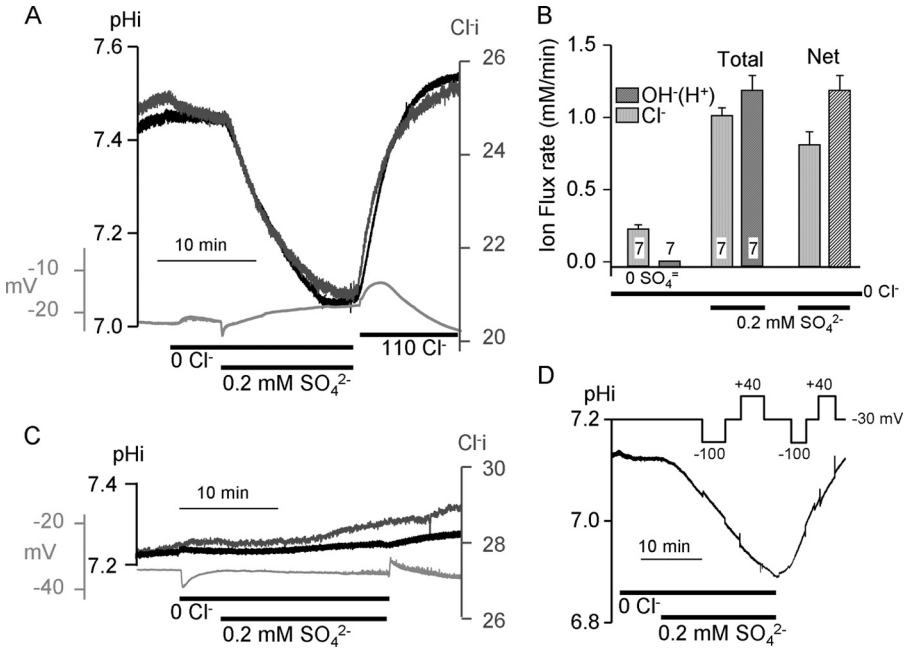

FIGURE 1. **Slc26a2 functions as an electroneutral $SO_4^{2-}/OH^-(H^+)/Cl^-$ exchanger.** pH_i (*dark traces*) and $Cl^-{}_i$ (*dark gray traces*) and membrane potential (*light gray traces*) were simultaneously recorded in Slc26a2 (*A*) or H_2O (*C*)-injected oocytes. Note that the membrane potential did not change following addition of SO_4^{2-}. *B*, averaged (mean ± S.E. of the indicated number of experiments) transport rates of Cl^- and $OH^-(H^+)$ in the presence and absence of 0.2 mM SO_4^{2-} were used to determine net transport (*rightmost columns*). *D*, pH_i was recorded while clamping membrane potential at −100 , +40, or −30 mV, as indicated.

Supplemental Fig. 1*A* shows that two consecutive injections of the oocytes with 13.8 nl of 100 mM HCl reduced pH_i and increased $Cl^-{}_i$. Similar determination in five experiments and using the pH_i and $Cl^-{}_i$ changes of the first injection resulted in a buffer capacity of 17.1 ± 2.2/pH unit, which is similar to that reported by others (33).

Modeling and Prediction of the Slc26a2 Transmembrane Domains Structure—The transmembrane sector of the mouse Slc26a2 model was generated using the Deepview Swiss-PDB viewer by Raw sequence fit of the Slc26a2 sequence (NCBI accession no. NP_031911) onto the putative Slc26a6 model previously generated by us based on structural similarity to the bacterial ClC-ec protein (29). The predicted binding site of DIDS on the Slc26a2 model was performed with the AutoDockVina software (34), according to software tutorial instructions. Briefly, the box grid determining the Slc26a2 region of binding was set using the AutoDockTools software with the following coordinates (center: $x = 0.472$, $y = 1.222$, $z = 0.472$) (size: $x = 30$, $y = 26$, $z = 24$). Exhaustiveness level was set to default. AutoDockTools was further used to select all rotatable bonds of the DIDS molecule. The AutoDockVina software generated nine different models, and herein we present the best model as ranked by the software with a predicted affinity of −8.9 kcal/mol for the binding of Slc26a2 and DIDS. The final model (cartoon and surface representations) was generated using PyMOL (Schrödinger, LLC).

RESULTS AND DISCUSSION

Slc26a2 Functions as an $SO_4^{2-}/2OH^-$, $SO_4^{2-}/2Cl^-$, and Possibly $SO_4^{2-}/OH^-/Cl^-$ Exchanger—Slc26a2-mediated net fluxes were assayed in *Xenopus* oocytes by measuring intracellular pH (pH_i) and Cl^- ($Cl^-{}_i$) and the membrane potential in the same oocytes. Fig. 1*A* shows that removal of extracellular Cl^- ($Cl^-{}_o$) had no effect on pH_i and the membrane potential with a slow rate of reduction in $Cl^-{}_i$. Exposing Slc26a2-expressing oocytes bathed in Cl^--free solution to 0.2 mM SO_4^{2-} resulted in a precipitous reduction in pH_i and $Cl^-{}_i$. Removal of $SO_4^{2-}{}_o$ with the concomitant addition of $Cl^-{}_o$ resulted in increased pH_i and $Cl^-{}_i$. Fig. 1*C* shows almost no change in $Cl^-{}_i$ and pH_i in water-injected oocytes under the same conditions.

Reduction in pH_i can be due to H^+ influx or OH^- efflux. Because some of the SO_4^{2-} transport is coupled to Cl^-, and the Cl^- coupling is affected by pH_o (see below), we will refer to the transported ion as OH^-, although we cannot distinguish between the transport of OH^- and H^+. The average Slc26a2-mediated SO_4^{2-}-coupled net Cl^- and OH^- transports are shown in Fig. 1*B* and indicate that under the conditions of Fig. 1*A* ~40% of SO_4^{2-} is transported in exchange for Cl^- and ~60% in exchange with OH^-. SO_4^{2-} transport is electroneutral, because it is not associated with a change in membrane potential (Fig. 1), and SO_4^{2-}-coupled OH^- (Fig. 1*D*) and Cl^- (not shown) fluxes are the same at membrane potentials of +40 and −100 mV. This indicates that the coupling stoichiometry of SO_4^{2-} exchange with Cl^- and OH^- is likely 1:2 with Slc26a2 functioning as $SO_4^{2-}/2OH^-$, $SO_4^{2-}/2Cl^-$ and possible $SO_4^{2-}/OH^-/Cl^-$ exchanger.

To further determine the relationship between SO_4^{2-} and Cl^- we measured the effect of $Cl^-{}_o$ on the apparent affinity for $SO_4^{2-}{}_o$. Fig. 2*A* shows an example of the protocol used for these experiments. Oocytes expressing Slc26a2 were exposed to solutions containing the desired $Cl^-{}_o$ (0, 5, 20 or 50 mM) and SO_4^{2-} concentration for 5 min to obtain the rate of OH^- efflux. Then the oocytes were incubated in Cl^--containing solution without SO_4^{2-} to extrude the SO_4^{2-} and recover pH_i before exposure to the subsequent SO_4^{2-} concentration. The plots in Fig. 2*B*

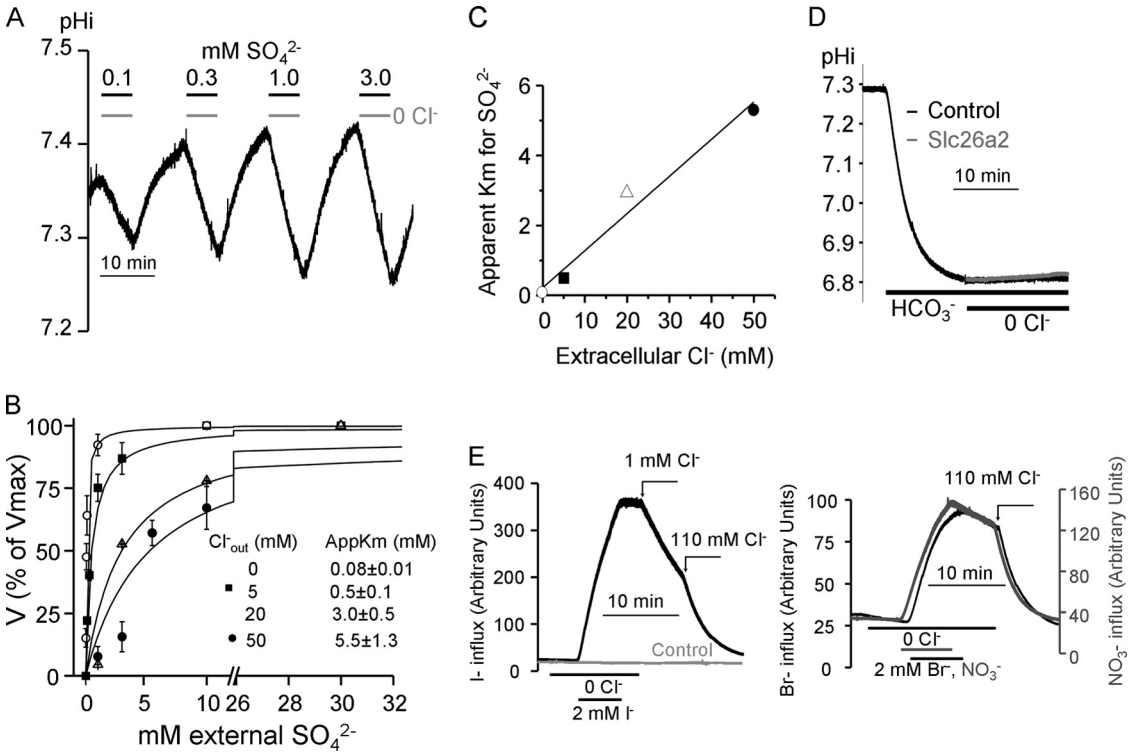

FIGURE 2. **Effect of Cl^-_o on Slc26a2-mediated $SO_4^{2-}{}_o/OH^-{}_i$ exchange.** *A*, Slc26a2-expressing oocytes were alternately perfused with a solution containing 110 mM Cl^- and Cl^--free solutions containing the indicated SO_4^{2-} concentrations for ~5 min. The plots in *B* are the relative average rates of OH^- fluxes as a function SO_4^{2-} at $Cl^-{}_o$ of 0 (○), 5 (■), 20 (△), and 50 (●) mM. The rates were normalized to the rate at 30 mM SO_4^{2-}, which was taken as 100%, and the plots were fitted to the Hill equation. The averages are the mean ± S.E. of 3–5 experiments at each $Cl^-{}_o$ concentration. The resulting apparent K_m values for SO_4^{2-} are plotted as a function of $Cl^-{}_o$ (*C*). *D*, control (H_2O-injected, *black trace*) and Slc26a2-expressing oocytes (*gray trace*) bathed in HCO_3^--buffered solution were exposed to Cl^--free solution at the indicated time to asses Cl^-/HCO_3^- exchange activity. In *E* the exchange of I^-, Br^-, and NO_3^- with $Cl^-{}_i$ was measured by incubating oocytes in Cl^--free solution containing 2 mM of I^- (*left traces*), Br^-, or NO_3^- (*right traces*). The influx was terminated by removal of the anions from the bath and anion efflux was initiated by addition of Cl^- to the bath. The lack or minimal anion efflux in the absence of $Cl^-{}_o$ indicates low net and exchange rate of the anions with OH^- and the rapid efflux of the anions upon addition of $Cl^-{}_o$ indicates fast exchange rate of the anions with Cl^-. The control in the *left panel* is representative of oocytes injected with H_2O.

obtained from these experiments were used to calculate the apparent K_m for SO_4^{2-} that were then plotted as a function of $Cl^-{}_o$ (Fig. 2*C*). The linear relationship in Fig. 2*C* indicates that $Cl^-{}_o$ competes with $SO_4^{2-}{}_o$ for interaction with the external substrate site. This competition is different from the non-saturating $Cl^-{}_o$ dependence reported for the isotopic exchange of $Cl^-{}_o$ with intracellular Cl^- ($Cl^-{}_i$) or intracellular oxalate (24). This may reflect the different dependence of $Cl^-{}_o$ of the half (exchange) and full turnover cycle (net) of transport by Slc26a2.

Many of the SLC26 transporters can transport HCO_3^- in exchange for Cl^- (9). However, Fig. 2*D* shows that Slc26a2 does not function as a Cl^-/HCO_3^- exchanger. The capacity of Slc26a2 to transport other anions, such as I^-, Br^- and NO_3^-, in addition to SO_4^{2-}, OH^- and Cl^- was further tested by measuring their intracellular concentration. Supplemental Fig. 1*B* shows that the resin used to detect Cl^- can also detect Br^- and NO_3^- ~10 times better than Cl^- and I^- ~100 times better than Cl^- (see also (29)). The *left panel* of Fig. 2*D* shows that exposing Slc26a2-expressing oocytes to Cl^--free solution containing 2 mM I^- resulted in a rapid influx of I^-. Removal of I^- in the absence of $Cl^-{}_o$ stopped the influx. To initiate I^- efflux it was necessary to add $Cl^-{}_o$, with as little as 1 mM $Cl^-{}_o$ resulting is nearly maximal rate of I^- efflux. Similar behavior was observed with Br^- and NO_3^- (Fig. 2*D*, *right panel*) and no I^- (Fig. 2*D*, *gray trace, left panel*), Br^- or NO_3^- (not shown) fluxes were observed in water-injected oocytes. These findings indicate that the Slc26a2 permeation pathway is not very selective and can accommodate I^-, Br^- and NO_3^- to mediate I^-/Cl^-, Br^-/Cl^- and NO_3^-/Cl^- exchange.

The Ratio of $SO_4^{2-}/2OH^-$ and $SO_4^{2-}/2Cl^-$ Exchange Is Determined by pH_o—Coupling of SO_4^{2-} transport to OH^- and Cl^- raised the question of how the availability of substrate would affect the coupling. We addressed this question by examining the effect of pH_i and pH_o on SO_4^{2-} transport. Fig. 3*A* shows example traces of the changes in pH_i (*left panel*) and of the $Cl^-{}_i$ (*right panel*) as a result of SO_4^{2-} transport at pH_o of 6.5 (*black traces*) and 8.2 (*gray traces*). The rates of OH^- and Cl^- influx and efflux under both conditions are summarized in Fig. 3*B*. The models in Fig. 3*B* show the direction of ion fluxes during SO_4^{2-} influx (*left*) and SO_4^{2-} efflux (*right*) and the *columns* show the associated $OH^-(H^+)$ and Cl^- fluxes at pH_o of 6.5 and 8.2. SO_4^{2-} influx is coupled to Cl^- and OH^- efflux, while SO_4^{2-} efflux initiated by removal of $SO_4^{2-}{}_o$ and addition of $Cl^-{}_o$ is coupled to Cl^- and OH^- influx. During SO_4^{2-} influx acidic pH_o increases OH^- efflux with low Cl^- efflux while alkaline pH_o has the opposite effect. On the other hand, during SO_4^{2-} efflux acidic pH_o inhibits OH^- efflux and increases Cl^- efflux while alkaline pH_o has the opposite effect.

Fig. 3*C* further illustrates the reciprocal effect of pH_o on OH^- and Cl^- fluxes. Exposing Slc26a2-expressing oocytes to a solu-

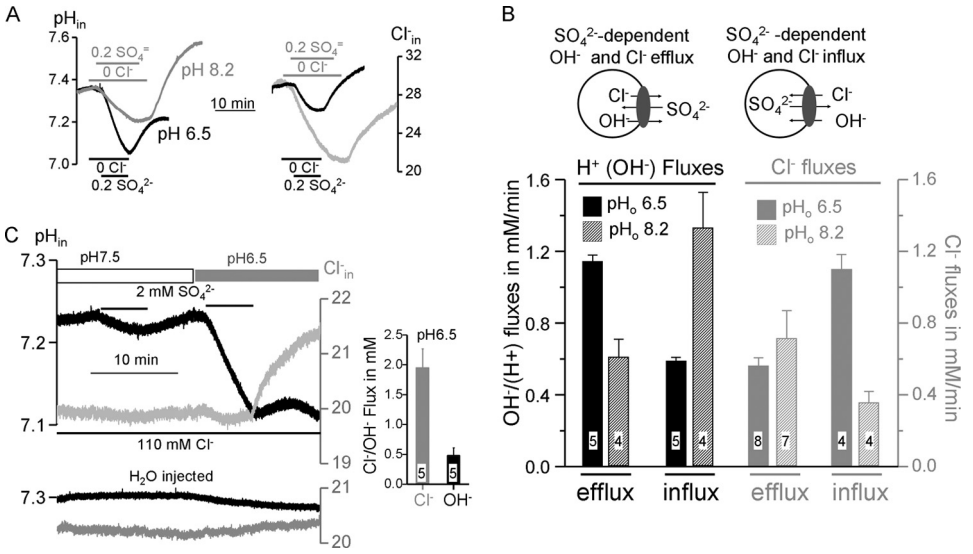

FIGURE 3. **Effect of pH$_o$ on $SO_4^{2-}{}_o$ influx and $SO_4^{2-}{}_i$ efflux.** *A*, example traces for measurement of pH$_i$ and $Cl^-{}_i$ in solutions buffered to pH$_o$ of 6.5 (*black traces*) or 8.2 (*gray traces*). The models in *B* show the direction of the fluxes and the average efflux and influx rates of $OH^-(H^+)$ (*dark columns*) and Cl^- (*gray columns*) fluxes are summarized in *B*. The results are the mean ± S.E. of the number of experiments listed in the columns. In *C* pH$_i$ and $Cl^-{}_i$ were measured at 110 mM $Cl^-{}_o$ and first at pH$_o$ of pH 7.5 and then at pH$_o$ of 6.5. The *columns* on the *right* show the average rates (mean ± S.E.) of Cl^- and OH^- influx at pH$_i$ of 6.5 upon removal of SO_4^{2-}, and the *lower traces* are example traces obtained in H_2O-injected oocytes.

tion buffered to pH 7.5 and containing 110 mM Cl^- and 2 mM SO_4^{2-} resulted in a reduction in pH$_i$ at a rate of ~0.18 ± 0.03 mM/min (n = 8), with no change in $Cl^-{}_i$. Removal of SO_4^{2-} resulted in recovery of pH$_i$. H_2O injected oocytes showed no response to SO_4^{2-}. Hence, at high $Cl^-{}_o$ and pH$_o$ of 7.4 all the Slc26a2-mediated $SO_4^{2-}{}_i$flux is mediated by $SO_4^{2-}/2OH^-$ exchange (or $SO_4^{2-}/2H^+$ cotransport). When the same oocytes were exposed to the same solution containing 110 Cl^- and 2 mM SO_4^{2-}, but now buffered to pH of 6.5, SO_4^{2-} uptake resulted in a large reduction in pH$_i$ with no change in $Cl^-{}_i$, while SO_4^{2-} efflux initiated by removal of $SO_4^{2-}{}_o$ resulted in a small increase in pH$_i$ and a large Cl^- influx (Fig. 3*C*). Thus, at low pH$_o$ SO_4^{2-} uptake is predominantly mediated by $SO_4^{2-}/2OH^-(2H^+)$ exchange, while SO_4^{2-} efflux is dominated by $SO_4^{2-}{}_i/Cl^-{}_o$ exchange.

The sulfate transported species can be SO_4^{2-} or HSO_3^-. Although we did not examine this in great detail, the results in Figs. 1–3 favor SO_4^{2-}. Thus, if the transported species is HSO_3^- then acidic pH$_o$ should markedly enhance Sulfate influx. Fig. 3*B* indicates that is not the case. Second, SO_4^{2-} efflux after removal of $SO_4^{2-}{}_o$ should be independent of pH$_o$ since pH$_o$ should have no effect of the transported SO_4^{2-} species. Again, this is not the case. Third, changes on pH$_o$ have the same effect on SO_4^{2-} and Ox^{2-} transport (see below), suggesting that the transport rate follows the pH gradient rather than substrate species.

Coupling of SO_4^{2-} transport to both Cl^- and OH^- may function to ensure SO_4^{2-} uptake under acidic and alkaline conditions. Slc26a2 is expressed in the luminal membrane of polarized cells (31, 35) that can be exposed to acidic and alkaline pH. In the stomach and synovial fluid pH is acidic (36, 37) and $SO_4^{2-}{}_o/2OH^-{}_i$ exchange mediates most SO_4^{2-} uptake. On the other hand, in secretory glands, like the pancreas (38) and salivary glands (39), luminal pH is alkaline, which inhibits $SO_4^{2-}{}_o/OH^-{}_i$ exchange (Fig. 3*B*) and most SO_4^{2-} uptake is by $SO_4^{2-}{}_o/2Cl^-{}_i$ exchange.

Regulation of Slc26a2 by $Cl^-{}_o$—While measuring net SO_4^{2-} efflux we noticed that removal of $SO_4^{2-}{}_i$ in the continuous absence of $Cl^-{}_o$ never resulted in SO_4^{2-} efflux, as would be expected from $SO_4^{2-}{}_i/2OH^-{}_o$ exchange. This is illustrated in the period bordered by the dashed box of Fig. 4*A*. However, addition of as little as 1 mM $Cl^-{}_o$ triggered a robust $SO_4^{2-}{}_i/2OH^-{}_o$ exchange and a small Cl^- influx (Fig. 4*A*, *period* marked by *gray box*). The dependence of the $SO_4^{2-}{}_i/2OH^-{}_o$ exchange rate of $Cl^-{}_o$ followed simple saturation curve with apparent K_m of 3.7 ± 0.9 mM (Fig. 4*B*). Activation of the exchange was not specific for Cl^-. Fig. 4*C* shows that 1 mM external Cl^-, Br^-, I^-, NO_3^- and SCN^- similarly activated $SO_4^{2-}{}_i/2OH^-{}_o$ exchange. Only 1 mM F^- did not activate the exchange (Fig. 4*C*), but actually inhibited the exchange initiated by the other anions (not shown).

The findings in Fig. 4 suggest that SO_4^{2-} transport by Slc26a2 is regulated by interaction of an anion with a regulatory site. The regulatory site is not selective for Cl^-, but because Cl^- is the major extracellular anion, Slc26a2 is likely regulated by $Cl^-{}_o$ interaction with the regulatory site. The $Cl^-{}_o$ regulatory site is likely different from the transport site since increased $Cl^-{}_o$ should increase $SO_4^{2-}{}_i/2Cl^-{}_o$ exchange while reducing $SO_4^{2-}{}_i/2OH^-{}_o$ exchange. However, the opposite is observed. Activation of Slc26a2-mediated $SO_4^{2-}{}_i/2OH^-{}_o$ by $Cl^-{}_o$ may be by stabilization of an active Slc26a2 conformation. However, the exact mechanism remains to be elucidated. The physiological significance of regulation of Slc26a2 activity by $Cl^-{}_o$ is not known at present. The Cl^- content in the GI tract is high in the range of 100–150 mM and is determined largely by acid secretion (40). On the other hand, urine Cl^- can be below 4 mM when prerenal azotemia occurs with metabolic alkalosis (41) and regulation of Slc26a2 by $Cl^-{}_o$ can become significant. In addition, the luminal membrane-localized Slc26a2 is exposed to variable Cl^- concentrations, as low Cl^- in ducts that absorb the Cl^-, such as the pancreatic (38) and salivary (32) ducts, the

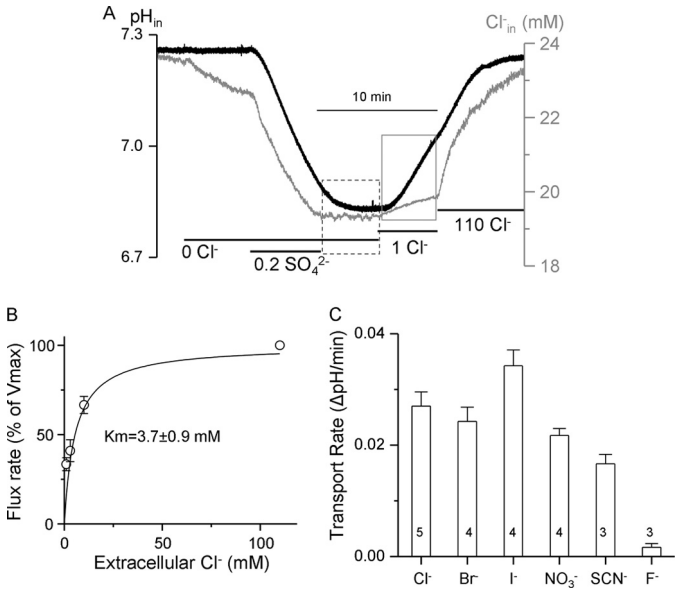

FIGURE 4. **Activation of Slc26a2-mediated $SO_4^{2-}{}_i/OH^-{}_o$ exchange by $Cl^-{}_o$.** *A*, example traces of $Cl^-{}_i$ (*black*) and pH_i (*gray*) in oocytes expressing Slc26a2. $SO_4^{2-}{}_i$ flux was terminated by removal of $SO_4^{2-}{}_o$ (*period bordered by dashed line*). SO_4^{2-} efflux did not start until the addition of 1 mM $Cl^-{}_o$ (*period bordered by gray square*), which triggered robust $SO_4^{2-}{}_i/OH^-{}_o$ exchange with minimal $SO_4^{2-}{}_i/Cl^-{}_o$ exchange. *B*, the relative rate of $SO_4^{2-}{}_i/OH^-{}_o$ exchange is plotted as a function of the activating $Cl^-{}_o$. The rates at each $Cl^-{}_o$ were normalized to the rate measured at 110 mM $Cl^-{}_o$, which was taken as 100%. The plot is the average of 3–5 experiments and fitted to the Hill equation. *C*, the protocol in *A* was used to measure activation of $SO_4^{2-}{}_i/OH^-{}_o$ exchange by 1 mM of the indicated anions (*period marked by gray square*). The results are mean ± S.E. of the number of experiments indicated in the *columns*.

intestine (42) and the vas deferens (43). One possibility is that SO_4^{2-} absorption take place only when there is some luminal Cl^-. Perhaps in Cl^- absorbing epithelia completion of Cl^- absorption may be used to signal termination of the SO_4^{2-} absorptive activity. Additionally, regulation by $Cl^-{}_o$ may be used to stop reverse Slc26a2 transport to prevent SO_4^{2-} loss by SO_4^{2-} efflux across the luminal membrane due to $SO_4^{2-}{}_i/2OH^-{}_o$ when luminal Cl^- becomes very low due to Cl^- absorption.

A Potential Slc26a2 Permeation Pathway—In a previous study we developed a model of the Slc26a6 transmembrane sector to search for motifs that determine the function of the electrogenic Slc26 transporters as coupled and uncoupled transporters (29). The modeling identified a glutamate (Glu^-) conserved in all Slc26 transporters that has the same orientation as Glu^- E148 in the Cl^- permeation pathway of the ClC transporters (44–47). Interestingly, a recent study utilized the predicted Slc26a6 model and the crystal structure of the Slc26a5 STAS domain to assemble a detailed putative structure of Slc26 transporters (48). This structure showed a surprising similarity to the low resolution structure of a bacterial Slc26 homologue obtained using SANS (small angle neutron scattering) method in terms of symmetry and size. Notably, this study suggested that Slc26 functions as a dimer, as was previously suggested based on the predicted similarity of Slc26a6 to the bacterial ClC-ec dimeric crystal structure. Therefore, assuming a similar overall architecture for Slc26 transporters, we thread the Slc26a2 transmembrane sector on the Slc26a6 model to determine the localization of the conserved Glu^- Glu^{417} (Fig. 5). Another purpose of the modeling was to identify additional determinants of the Slc26a2 ion permeation pathway and perhaps the extracellular Cl^- regulatory site. The motif GSGIP was identified as a potential anion (Cl^-) binding site that is conserved in the ClC transporters (44, 49). Mutations of residues within this motif altered ionic selectivity and coupling in the yeast and mammalian ClCs (50, 51). We searched for a similar motif in the Slc26 transporters. Although identical motif is not present in the Slc26 transporters, supplemental Fig. 2 shows the presence of the well conserved sequence GF*XX*P. The structural model in Fig. 5 shows the predicted localization of the Slc26a2 conserved Glu^- Glu^{417} and phenylalanine Phe^{368} and of a potential DIDS binding site.

To test the prediction in Fig. 5 we first determined the sensitivity of Slc26a2 to DIDS. Fig. 6*A* shows that 50 μM DIDS completely inhibited SO_4^{2-}-driven OH^-(H^+) efflux and most of the SO_4^{2-}-driven Cl^- efflux. The residual DIDS-insensitive Cl^- efflux is likely not mediated by Slc26a2 but by a DIDS-insensitive transporter native to the oocytes. Fig. 6*B* shows that DIDS inhibited SO_4^{2-} efflux when added after SO_4^{2-} uptake. Also in this case DIDS completely inhibited OH^-(H^+) influx, but with a residual Cl^- influx. Similar results were obtained with 10 and 50 μM DIDS, indicating that the DIDS sensitivity of Slc26a2 is in the same range of that reported for Slc26a6 (52). Fig. 6*C* summarizes the rates of OH^- and Cl^- fluxes in the absence and presence of SO_4^{2-} and DIDS, indicating that at pH_o of 7.5 and the absence of $Cl^-{}_o$ ~60% of SO_4^{2-} uptake is coupled to OH^- efflux and 40% to Cl^- efflux. Fig. 6*D* test another prediction of the model in Fig. 5 by neutralizing (Slc26a2(E417A)) or reversing (Slc26a2(E417K)) the charge of the conserved Glu^{417}. Both mutations eliminated SO_4^{2-} (Fig. 6*D*) and I^- (not shown) transport activity. Inhibition of transport was not due to altered trafficking of the mutants to the plasma membrane (Fig. 6*E*).

The sequence GF*XX*P is predicted to be in the extracellular loop between transmembrane domains (TMDs) 7 and 8, with Phe^{368} predicted to be in the entrance of the permeation pathway (Fig. 5). The mutations G367A and P371A had no effect on SO_4^{2-} transport or its coupling to Cl^- and OH^- (not shown). However the F368A mutation had multiple effects. Fig. 7*A* shows that Slc26a2(F368A) is ~50% less active than wild-type Slc26a2 in exchanging SO_4^{2-} for OH^- (*left traces*) and Cl^- (*right traces*). Most notably, the F368A mutation increased the apparent affinity of Slc26a2 for SO_4^{2-} by ~8-fold to reduce the apparent K_m for $SO_4^{2-}{}_o$ from 79 ± 7 to 9.7 ± 0.7 μM. Unexpectedly from competition between $SO_4^{2-}{}_o$ and $Cl^-{}_o$ (Fig. 2), the F368A mutation increased the apparent K_m for inhibition of SO_4^{2-} uptake by $Cl^-{}_o$ from 26 to 50 mM (Fig. 7*C*). Hence, Phe^{368} appears to control the access of SO_4^{2-} and Cl^- to the permeation pathway. Interestingly, Fig. 7*D* shows that the F368A mutation had no effect of the apparent affinity for the $Cl^-{}_o$ regulatory site that activates $SO_4^{2-}{}_i/OH^-{}_o$ exchange. This finding provides the strongest evidence that inhibition of SO_4^{2-} uptake by $Cl^-{}_o$ (Figs. 4*B* and 7*C*) and activation of $SO_4^{2-}{}_i/OH^-{}_o$ exchange by $Cl^-{}_o$ probably involves interaction of $Cl^-{}_o$ with two separate sites.

The findings in Fig. 7, *A*–*C* provide additional evidence for the importance of the GSGIP or the GF*XX*P motifs in the function of the Cl^- transporters, in addition to the two additional

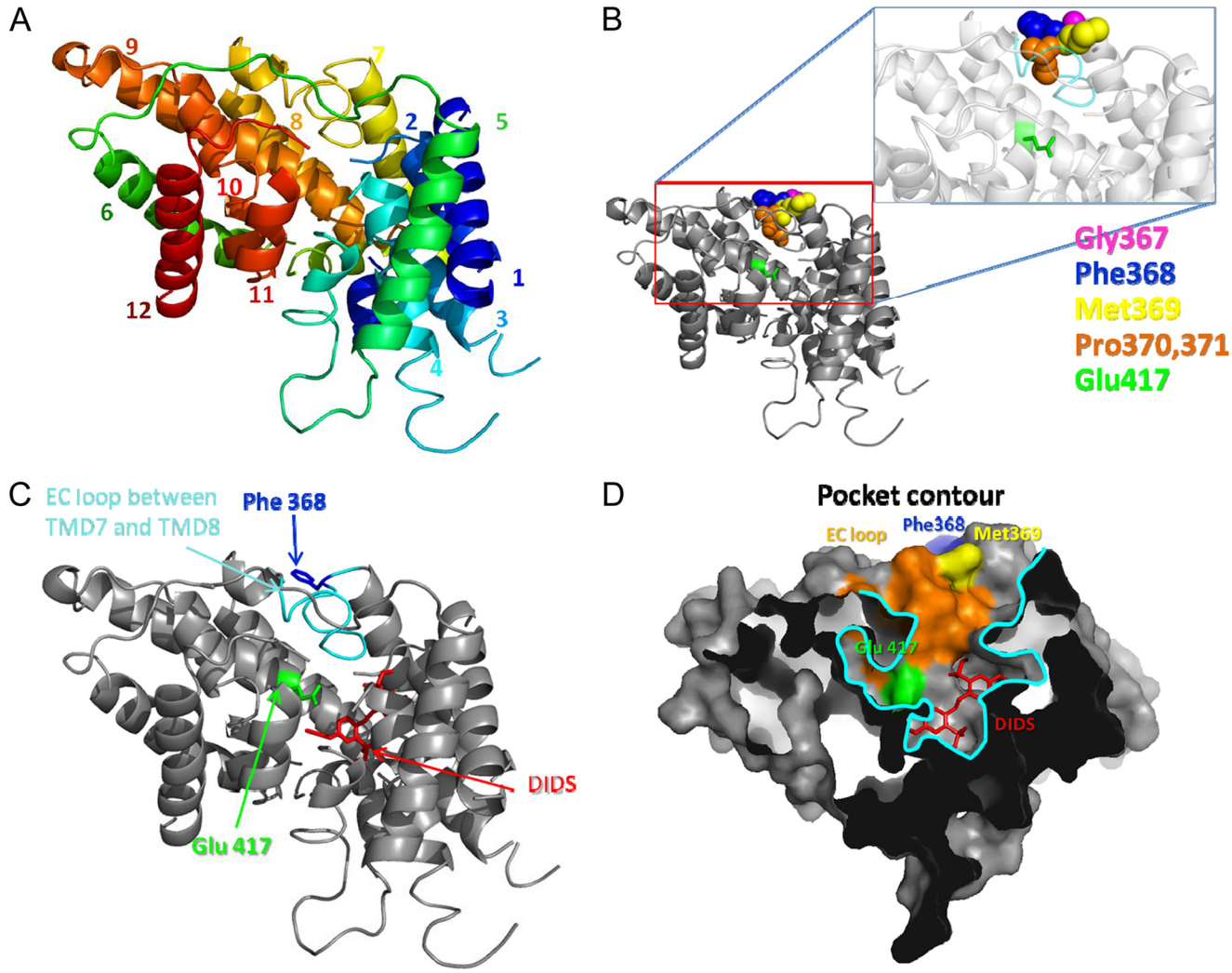

FIGURE 5. ***In silico* model of the putative structure of the Slc26a2 TMDs.** The model was derived by threading the TMD sector of Slc26a2 on the TMDs of Slc26a6 reported before (29) (see "Experimental Procedures"). *A*, shows the predicted position of the 12 transmembrane helices of Slc26a2. *B*, shows the space filling of the GFMPG sequence. Highlighted in *C* are the positions of the extracellular loop located between TMDs 7 and 8 (*light blue*), the conserved phenylalanine Phe^{368} (*blue*), the conserved Glu^{-} Glu^{417} (*green*), and the putative position of DIDS binding site (*red*). *D*, illustrates a cross-section (~20 Å) through the surface representation of the putative Slc26a2 revealing a potential binding cavity. Interestingly, Glu^{-} 417 (*green*) and the EC loop (*orange*) are constituents of the binding pocket (*outlined in cyan*) in which the inhibitor DIDS (*red*) is also bound.

GXXXP motifs that participate in Cl^- transport in the bacterial ClCs (44). The bacterial ClC-ec1 crystal structure shows that the permeation pathway has three Cl^- interacting sites (44–46, 49). Ser^{107} and Gly^{108} in the GSGIP motif coordinate the Cl^- ion in the internal substrate site, and the side chain of Ser^{107} participates in binding of the middle Cl^- (45, 49). In Slc26a2 Phe^{368} appears to control the affinity for the substrate (SO_4^{2-}), suggesting that Phe^{368} may participate in the access of SO_4^{2-} to the permeation pathway or in shaping the external SO_4^{2-} binding site. The increased apparent affinity for SO_4^{2-} and reduced apparent affinity for Cl^- by the F368A mutation suggests that Phe^{368} may hinder access of SO_4^{2-} and facilitate access of Cl^- to the permeation pathway or reduces the time SO_4^{2-} spends in the external binding site on its way across the plasma membrane. Perhaps this is necessary to allow $SO_4^{2-}{}_i/Cl^-{}_o$ exchange at high $SO_4^{2-}{}_i$ when SO_4^{2-} efflux is required. Irrespective of the exact role of Phe^{368}, the present findings further support the notion of similarities between the ClC and SLC26 transporters permeation pathways and that the opening of the permeation pathway is situated in the region of TMDs 7 and 8.

Properties of Slc26a2-mediated Oxalate Transport—Slc26a2 was reported to transport Oxalate (Ox^{2-}) by mediate Ox^{2-}/SO_4^{2-} exchange (8, 24–26, 28) and that Ox^{2-}/SO_4^{2-} exchange is 10 times slower than SO_4^{2-}/Cl^- exchange (24). However, the properties and mode of Ox^{2-} transport and the capacity of net Ox^{2-} transport by Slc26a2 are not known. We set to estimate net Ox^{2-} transport by measuring Ox^{2-}-mediated OH^- and Cl^- fluxes. Fig. 8*A* shows that Slc26a2 mediates net $Ox^{2-}{}_o/OH^-{}_i$ and $Ox^{2-}{}_o/Cl^-{}_i$ exchange in oocytes bathed in Cl^--free solution containing 1 mM Ox^{2-}, pH 7.5. Removal of Ox^{2-} was not followed by Ox^{2-} efflux until the addition of 1 mM $Cl^-{}_o$ to activate the efflux. Importantly, addition of 1 mM $Cl^-{}_o$ resulted in minimal $Ox^{2-}{}_i/Cl^-{}_o$ exchange but near maximal $Ox^{2-}{}_i/OH^-{}_o$ exchange. Increasing $Cl^-{}_o$ to 110 mM caused a small additional increase in $Ox^{2-}{}_i/OH^-{}_o$ exchange and modest $Ox^{2-}{}_i/Cl^-{}_o$ exchange. As expected, Fig. 8*B* shows that

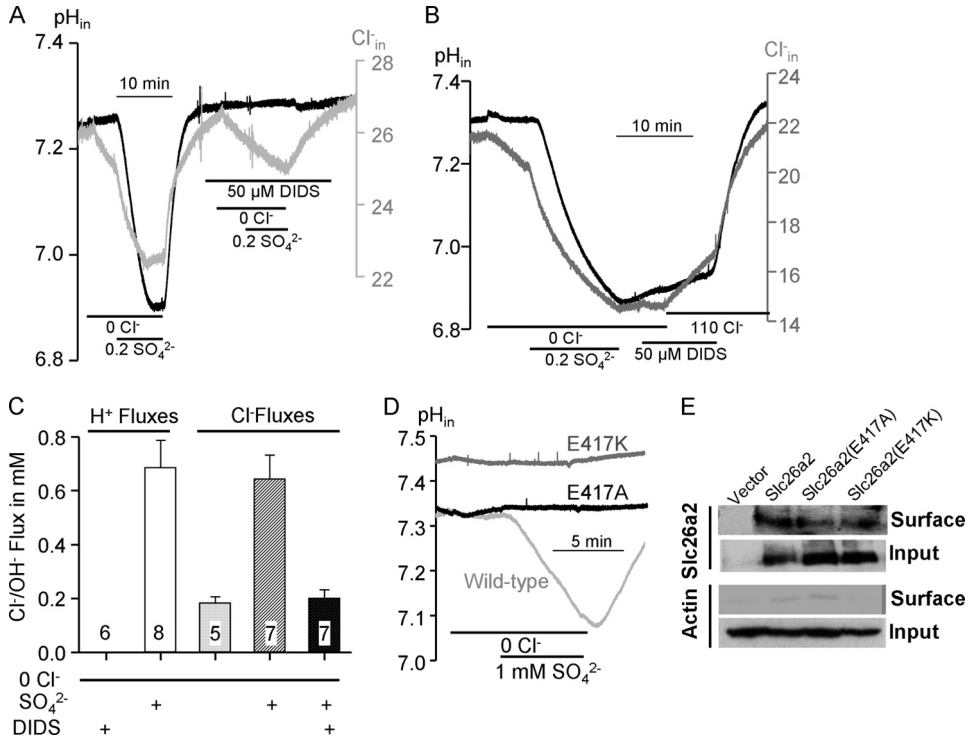

FIGURE 6. **Inhibition of Slc26a2 by DIDS and by mutations of Glu^{417}.** Example traces depicting inhibition of $SO_4^{2-}{}_i$ flux (*A*) and SO_4^{2-} efflux (*B*) by 50 μM DIDS. Note the complete inhibition of the coupled OH^- but not of Cl^- fluxes. *C*, the average rates (mean ± S.E. of the indicated number of experiments) of OH^- and Cl^- fluxes. In *D* shown are examples of oocytes expressing either wild-type Slc26a2, Slc26a2(E417A), or Slc26a2(E417K) that were used to measure the SO_4^{2-}-associated OH^- and Cl^- fluxes. *E*, shows the surface expression of Slc26a2 and mutants with actin used as a control for the biotinylation.

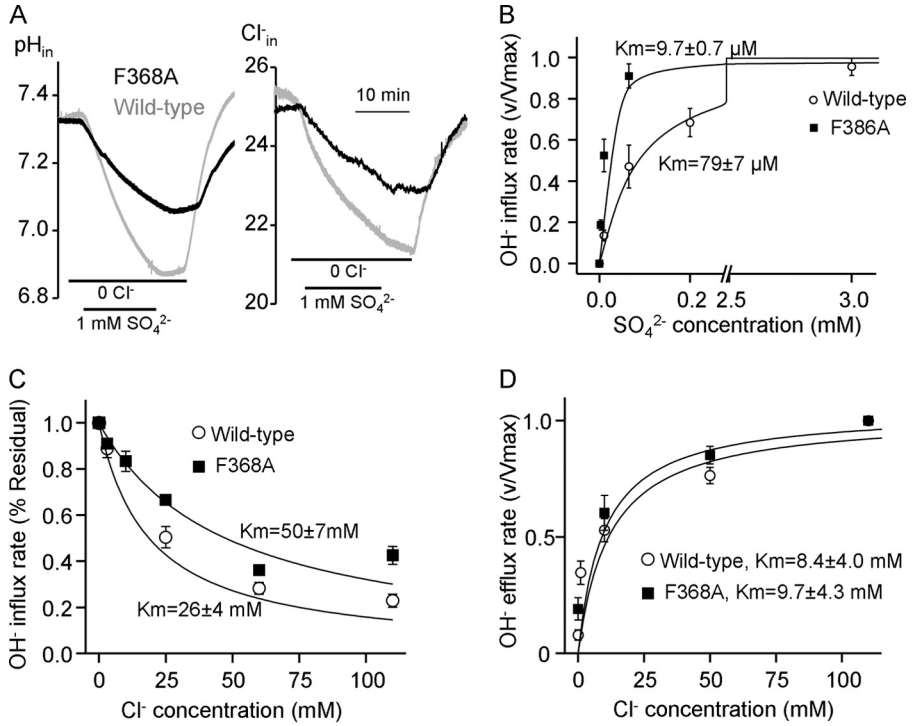

FIGURE 7. **Phe^{368} in Slc26a2 permeation pathway.** *A*, example traces for pH_i and $Cl^-{}_i$ measurement in oocytes expressing either wild-type (*gray traces*) or Slc26a2(F368A) (*black traces*). This protocol was used to monitor Slc26a2-mediated the SO_4^{2-} dependence of $SO_4^{2-}{}_o/OH^-{}_i$ exchange (*B*) and inhibition of the exchange by $Cl^-{}_o$ (*C*). $SO_4^{2-}{}_i/OH^-{}_o$ exchange was used to monitor activation of the reverse exchange by $Cl^-{}_o$ (*D*). All plots (*B–D*) were fitted to the Hill equation, and K_m values are given as mean ± S.E.

reducing pH_o to 6.5 increased the rate of $Ox^{2-}{}_o/OH^-{}_i$ exchange and increasing pH_o to 8.5 inhibited the $Ox^{2-}{}_o/OH^-{}_i$ exchange. Fig. 8*C* shows the opposite effect of pH_o on the $Ox^{2-}{}_i/OH^-{}_o$ exchange. Finally, the F368A mutation increased the apparent affinity for Ox^{2-} and reduced the apparent K_m for Ox^{2-} from 90 ± 12 to 50 ± 8 μM. Although this was not as

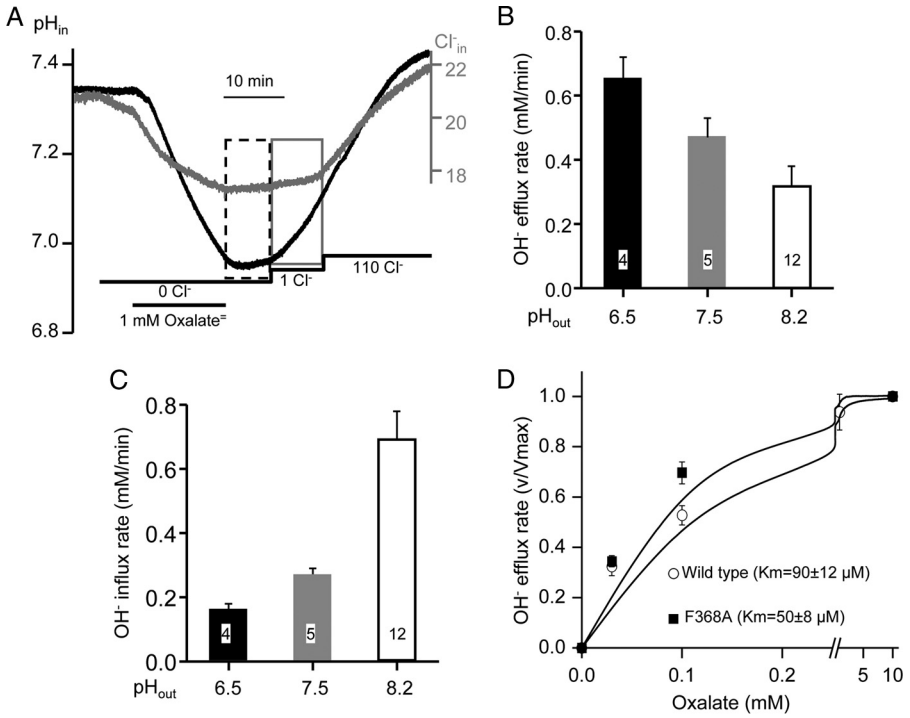

FIGURE 8. **Properties of Slc26a2-mediated oxalate (Ox^{2-}) transport.** *A*, example traces of the Slc26a2-mediated OH^- (*black trace*) and Cl^- (*gray trace*) efflux in response to addition of 1 mM $Ox^{2-}{}_o$ to Cl^--free solution at pH 7.5. Removal of $Ox^{2-}{}_o$ terminated the influx (*dashed box*) and addition of 1 mM $Cl^-{}_o$ was required to initiate $Ox^{2-}{}_i/OH^-{}_o$ exchange (*gray box*) with minimal $Ox^{2-}{}_i/Cl^-{}_o$ exchange. *B* and *C*, effect of pH_o of Ox^{2-} fluxes was as in *A*, except that the Ox^{2-} efflux was initiated by the addition of 110 mM $Cl^-{}_o$ and pH_o was set at 6.5 (*dark columns*), 7.5 (*gray columns*), or 8.2 (*empty columns*). The results are the mean ± S.E. of the number of experiments indicated in the *columns*. *D*, the dependence of $Ox^{2-}{}_o/OH^-{}_i$ exchange on $Ox^{2-}{}_o$ concentrations was measured with wild-type Slc26a2 (○) and Slc26a2(F368A) (■). The apparent K_m values are given as the mean ± S.E. of 4–5 experiments.

prominent as the increased apparent affinity for SO_4^{2-} (Fig. 7), it was in the same direction. The results in Fig. 8, *A–D* indicate that the properties of Ox^{2-} transport closely resemble those of SO_4^{2-} transport, although at the same conditions the Ox^{2-} transport rate was ~50% slower than the SO_4^{2-} transport rate.

In summary, the present study reports the mechanism of SO_4^{2-} and Ox^{2-} transport by Slc26a2. Both anions are transported in exchange for Cl^- and OH^- or by cotransport with H^+. Based on the rate of the coupled $OH^-(H^+)$ fluxes in the absence of $Cl^-{}_o$ and at substrate concentration of 1 mM, net SO_4^{2-} transport by Slc26a2 is about twice faster than net Ox^{2-} transport. Under normal conditions plasma oxalate is in the micromolar range and even in patients with primary hyperoxaluria plasma oxalate is around 40 μM (53). Moreover, although Slc26a2 is expressed at high level in the luminal membrane of colonic crypts (21), SO_4^{2-} in the colon can be in the millimolar range both in human (54) and animals (55) that will favor SO_4^{2-} uptake by Slc26a2. Indeed, the colon is a major site of SO_4^{2-} absorption (54, 56) that is likely mediated by Slc26a2. Similarly, although Slc26a2 is expressed in the proximal tubule luminal membrane (31), SO_4^{2-} concentration in the proximal tubule is in the millimolar range, and although the role of Slc26a2 in the kidney is not know, if any it is likely to function mainly as an SO_4^{2-} transporter (8). The only possible scenario where Slc26a2 can affect Ox^{2-} homeostasis is by mediating Ox^{2-} secretion in exchange for external SO_4^{2-} when external Cl^- is low and pH is high. Even then, this process will be inhibited by the high cytoplasmic Cl^- typical of epithelia and by intracellular SO_4^{2-}. Thus Slc26a2 is not likely to play a major role in oxalate metabolism in the colon or the kidney.

The permeation pathway includes the conserved SLC26 transporter Glu^- and may lay between TMD7 and TMD8, where a phenylalanine conserved in the loop predicted to connect the TMDs may control SO_4^{2-} and Cl^- access to the permeation pathway. As yet, mutations of these residues, or even in the vicinity of these residues, have not been found in patients with diastrophic dysplasia (57). This is most likely because Slc26a2 is an essential gene and the mutations that markedly affect Slc26a2 activity may not be compatible with life. Indeed, analysis of several disease causing Slc26a2 mutations showed retention of some SO_4^{2-} transport capacity by the mutants and a good correlation between loss of SO_4^{2-} transport and disease severity (25, 26). The coupling of SO_4^{2-} transport to both OH^- and Cl^- likely serves to ensure transport at both acidic pH when most SO_4^{2-} uptake is mediated by $SO_4^{2-}/2OH^-$ exchange and alkaline pH when most SO_4^{2-} uptake is mediated by $SO_4^{2-}/2Cl^-$ exchange. Slc26a2 is also regulated by an extracellular anion binding site different from the transport site, the physiological function of which remains to be determined, although it may control SO_4^{2-} uptake when $Cl^-{}_o$ is very low.

REFERENCES

1. Neel, N. F., Schutyser, E., Sai, J., Fan, G. H., and Richmond, A. (2005) Chemokine receptor internalization and intracellular trafficking. *Cytokine Growth Factor Rev.* **16,** 637–658
2. Alnouti, Y. (2009) Bile acid sulfation. A pathway of bile acid elimination and detoxification. *Toxicol. Sci.* **108,** 225–246
3. Gorsi, B., and Stringer, S. E. (2007) Tinkering with heparan sulfate sulfation to steer development. *Trends Cell Biol.* **17,** 173–177
4. Nakato, H., and Kimata, K. (2002) Heparan sulfate fine structure and specificity of proteoglycan functions. *Biochim. Biophys. Acta* **1573,** 312–318

5. Habuchi, O. (2000) Diversity and functions of glycosaminoglycan sulfotransferases. *Biochim. Biophys. Acta* **1474,** 115–127
6. Stone, M. J., Chuang, S., Hou, X., Shoham, M., and Zhu, J. Z. (2009) Tyrosine sulfation. An increasingly recognised post-translational modification of secreted proteins. *N. Biotechnol.* **25,** 299–317
7. Elgavish, A., and Meezan, E. (1991) Sulfation by human lung fibroblasts: SO4(2-) and sulfur-containing amino acids as sources for macromolecular sulfation. *Am. J. Physiol.* **260,** L450-L456
8. Markovich, D., and Aronson, P. S. (2007) Specificity and regulation of renal sulfate transporters. *Annu. Rev. Physiol.* **69,** 361–375
9. Dorwart, M. R., Shcheynikov, N., Yang, D., and Muallem, S. (2008) The solute carrier 26 family of proteins in epithelial ion transport. *Physiology* **23,** 104–114
10. Ohana, E., Yang, D., Shcheynikov, N., and Muallem, S. (2009) Diverse transport modes by the solute carrier 26 family of anion transporters. *J. Physiol.* **587,** 2179–2185
11. Superti-Furga, A., Hästbacka, J., Wilcox, W. R., Cohn, D. H., van der Harten, H. J., Rossi, A., Blau, N., Rimoin, D. L., Steinmann, B., Lander, E. S., and Gitzelmann, R. (1996) Achondrogenesis type IB is caused by mutations in the diastrophic dysplasia sulphate transporter gene. *Nat. Genet.* **12,** 100–102
12. Hästbacka, J., de la Chapelle, A., Mahtani, M. M., Clines, G., Reeve-Daly, M. P., Daly, M., Hamilton, B. A., Kusumi, K., Trivedi, B., and Weaver, A. (1994) The diastrophic dysplasia gene encodes a novel sulfate transporter: positional cloning by fine-structure linkage disequilibrium mapping. *Cell* **78,** 1073–1087
13. Höglund, P., Haila, S., Socha, J., Tomaszewski, L., Saarialho-Kere, U., Karjalainen-Lindsberg, M. L., Airola, K., Holmberg, C., de la Chapelle, A., and Kere, J. (1996) Mutations of the down-regulated in adenoma (DRA) gene cause congenital chloride diarrhoea. *Nat. Genet.* **14,** 316–319
14. Everett, L. A., Glaser, B., Beck, J. C., Idol, J. R., Buchs, A., Heyman, M., Adawi, F., Hazani, E., Nassir, E., Baxevanis, A. D., Sheffield, V. C., and Green, E. D. (1997) Pendred syndrome is caused by mutations in a putative sulphate transporter gene (PDS). *Nat. Genet.* **17,** 411–422
15. Liu, X. Z., Ouyang, X. M., Xia, X. J., Zheng, J., Pandya, A., Li, F., Du, L. L., Welch, K. O., Petit, C., Smith, R. J., Webb, B. T., Yan, D., Arnos, K. S., Corey, D., Dallos, P., Nance, W. E., and Chen, Z. Y. (2003) Prestin, a cochlear motor protein, is defective in non-syndromic hearing loss. *Hum. Mol. Genet.* **12,** 1155–1162
16. Touré, A., Lhuillier, P., Gossen, J. A., Kuil, C. W., Lhôte, D., Jégou, B., Escalier, D., and Gacon, G. (2007) The testis anion transporter 1 (Slc26a8) is required for sperm terminal differentiation and male fertility in the mouse. *Hum. Mol. Genet.* **16,** 1783–1793
17. Jiang, Z., Asplin, J. R., Evan, A. P., Rajendran, V. M., Velazquez, H., Nottoli, T. P., Binder, H. J., and Aronson, P. S. (2006) Calcium oxalate urolithiasis in mice lacking anion transporter Slc26a6. *Nat. Genet.* **38,** 474–478
18. Wang, Y., Soyombo, A. A., Shcheynikov, N., Zeng, W., Dorwart, M., Marino, C. R., Thomas, P. J., and Muallem, S. (2006) Slc26a6 regulates CFTR activity *in vivo* to determine pancreatic duct HCO_3^- secretion. Relevance to cystic fibrosis. *EMBO J.* **25,** 5049–5057
19. Shcheynikov, N., Yang, D., Wang, Y., Zeng, W., Karniski, L. P., So, I., Wall, S. M., and Muallem, S. (2008) The Slc26a4 transporter functions as an electroneutral Cl-/I-/HCO_3^- exchanger. Role of Slc26a4 and Slc26a6 in I- and HCO_3^- secretion and in regulation of CFTR in the parotid duct. *J. Physiol.* **586,** 3813–3824
20. Forlino, A., Piazza, R., Tiveron, C., Della Torre, S., Tatangelo, L., Bonafè, L., Gualeni, B., Romano, A., Pecora, F., Superti-Furga, A., Cetta, G., and Rossi, A. (2005) A diastrophic dysplasia sulfate transporter (SLC26A2) mutant mouse. Morphological and biochemical characterization of the resulting chondrodysplasia phenotype. *Hum. Mol. Genet.* **14,** 859–871
21. Haila, S., Hästbacka, J., Böhling, T., Karjalainen-Lindsberg, M. L., Kere, J., and Saarialho-Kere, U. (2001) SLC26A2 (diastrophic dysplasia sulfate transporter) is expressed in developing and mature cartilage but also in other tissues and cell types. *J. Histochem. Cytochem.* **49,** 973–982
22. Ballhausen, D., Bonafè, L., Terhal, P., Unger, S. L., Bellus, G., Classen, M., Hamel, B. C., Spranger, J., Zabel, B., Cohn, D. H., Cole, W. G., Hecht, J. T., and Superti-Furga, A. (2003) Recessive multiple epiphyseal dysplasia (rMED). Phenotype delineation in eighteen homozygotes for DTDST mutation R279W. *J. Med. Genet.* **40,** 65–71
23. Superti-Furga, A., Rossi, A., Steinmann, B., and Gitzelmann, R. (1996) A chondrodysplasia family produced by mutations in the diastrophic dysplasia sulfate transporter gene. Genotype/phenotype correlations. *Am. J. Med. Genet.* **63,** 144–147
24. Heneghan, J. F., Akhavein, A., Salas, M. J., Shmukler, B. E., Karniski, L. P., Vandorpe, D. H., and Alper, S. L. (2010) Regulated transport of sulfate and oxalate by SLC26A2/DTDST. *Am. J. Physiol. Cell Physiol.* **298,** C1363-C1375
25. Karniski, L. P. (2001) Mutations in the diastrophic dysplasia sulfate transporter (DTDST) gene. Correlation between sulfate transport activity and chondrodysplasia phenotype. *Hum. Mol. Genet.* **10,** 1485–1490
26. Karniski, L. P. (2004) Functional expression and cellular distribution of diastrophic dysplasia sulfate transporter (DTDST) gene mutations in HEK cells. *Hum. Mol. Genet.* **13,** 2165–2171
27. Superti-Furga, A., Neumann, L., Riebel, T., Eich, G., Steinmann, B., Spranger, J., and Kunze, J. (1999) Recessively inherited multiple epiphyseal dysplasia with normal stature, club foot, and double layered patella caused by a DTDST mutation. *J. Med. Genet.* **36,** 621–624
28. Satoh, H., Susaki, M., Shukunami, C., Iyama, K., Negoro, T., and Hiraki, Y. (1998) Functional analysis of diastrophic dysplasia sulfate transporter. Its involvement in growth regulation of chondrocytes mediated by sulfated proteoglycans. *J. Biol. Chem.* **273,** 12307–12315
29. Ohana, E., Shcheynikov, N., Yang, D., So, I., and Muallem, S. (2011) Determinants of coupled transport and uncoupled current by the electrogenic SLC26 transporters. *J. Gen. Physiol.* **137,** 239–251
30. Ko, S. B., Shcheynikov, N., Choi, J. Y., Luo, X., Ishibashi, K., Thomas, P. J., Kim, J. Y., Kim, K. H., Lee, M. G., Naruse, S., and Muallem, S. (2002) A molecular mechanism for aberrant CFTR-dependent HCO_3^- transport in cystic fibrosis. *EMBO J.* **21,** 5662–5672
31. Chapman, J. M., and Karniski, L. P. (2010) Protein localization of SLC26A2 (DTDST) in rat kidney. *Histochem. Cell Biol.* **133,** 541–547
32. Melvin, J. E., Yule, D., Shuttleworth, T., and Begenisich, T. (2005) Regulation of fluid and electrolyte secretion in salivary gland acinar cells. *Annu. Rev. Physiol.* **67,** 445–469
33. Becker, H. M., Bröer, S., and Deitmer, J. W. (2004) Facilitated lactate transport by MCT1 when coexpressed with the sodium bicarbonate cotransporter (NBC) in *Xenopus* oocytes. *Biophys. J.* **86,** 235–247
34. Trott, O., and Olson, A. J. (2010) AutoDock Vina. Improving the speed and accuracy of docking with a new scoring function, efficient optimization, and multithreading. *J. Comput. Chem.* **31,** 455–461
35. Kujala, M., Hihnala, S., Tienari, J., Kaunisto, K., Hästbacka, J., Holmberg, C., Kere, J., and Höglund, P. (2007) Expression of ion transport-associated proteins in human efferent and epididymal ducts. *Reproduction* **133,** 775–784
36. Treuhaft, P. S., and McCarty, D. J. (1971) Synovial fluid pH, lactate, oxygen and carbon dioxide partial pressure in various joint diseases. *Arthritis Rheum.* **14,** 475–484
37. Sachs, G. (2003) Physiology of the parietal cell and therapeutic implications. *Pharmacotherapy* **23,** 68S-73S
38. Steward, M. C., Ishiguro, H., and Case, R. M. (2005) Mechanisms of bicarbonate secretion in the pancreatic duct. *Annu. Rev. Physiol.* **67,** 377–409
39. Catalán, M. A., Scott-Anne, K., Klein, M. I., Koo, H., Bowen, W. H., and Melvin, J. E. (2011) Elevated incidence of dental caries in a mouse model of cystic fibrosis. *PLoS One* **6,** e16549
40. Guyton, A. C., and Hall, J. E. (2006) *Textbook of Medical Physiology*, 11th Ed., Elsevier Saunders, Philadelphia
41. Anderson, R. J., Gabow, P. A., and Gross, P. A. (1984) Urinary chloride concentration in acute renal failure. *Miner. Electrolyte Metab.* **10,** 92–97
42. Kato, A., and Romero, M. F. (2011) Regulation of electroneutral NaCl absorption by the small intestine. *Annu. Rev. Physiol.* **73,** 261–281
43. Xu, W. M., Shi, Q. X., Chen, W. Y., Zhou, C. X., Ni, Y., Rowlands, D. K., Yi Liu, G., Zhu, H., Ma, Z. G., Wang, X. F., Chen, Z. H., Zhou, S. C., Dong, H. S., Zhang, X. H., Chung, Y. W., Yuan, Y. Y., Yang, W. X., and Chan, H. C. (2007) Cystic fibrosis transmembrane conductance regulator is vital to sperm fertilizing capacity and male fertility. *Proc. Natl. Acad. Sci. U.S.A.* **104,** 9816–9821

44. Dutzler, R., Campbell, E. B., Cadene, M., Chait, B. T., and MacKinnon, R. (2002) X-ray structure of a ClC chloride channel at 3.0 A reveals the molecular basis of anion selectivity. *Nature* **415,** 287–294
45. Feng, L., Campbell, E. B., Hsiung, Y., and MacKinnon, R. (2010) Structure of a eukaryotic CLC transporter defines an intermediate state in the transport cycle. *Science* **330,** 635–641
46. Accardi, A., and Miller, C. (2004) Secondary active transport mediated by a prokaryotic homologue of ClC Cl^- channels. *Nature* **427,** 803–807
47. Picollo, A., and Pusch, M. (2005) Chloride/proton antiporter activity of mammalian CLC proteins ClC-4 and ClC-5. *Nature* **436,** 420–423
48. Compton, E. L., Karinou, E., Naismith, J. H., Gabel, F., and Javelle, A. (2011) Low resolution structure of a bacterial SLC26 transporter reveals dimeric stoichiometry and mobile intracellular domains. *J. Biol. Chem.* **286,** 27058–27067
49. Faraldo-Gómez, J. D., and Roux, B. (2004) Electrostatics of ion stabilization in a ClC chloride channel homologue from *Escherichia coli*. *J. Mol. Biol.* **339,** 981–1000
50. Bergsdorf, E. Y., Zdebik, A. A., and Jentsch, T. J. (2009) Residues important for nitrate/proton coupling in plant and mammalian CLC transporters. *J. Biol. Chem.* **284,** 11184–11193
51. Zdebik, A. A., Zifarelli, G., Bergsdorf, E. Y., Soliani, P., Scheel, O., Jentsch, T. J., and Pusch, M. (2008) Determinants of anion-proton coupling in mammalian endosomal CLC proteins. *J. Biol. Chem.* **283,** 4219–4227
52. Shcheynikov, N., Wang, Y., Park, M., Ko, S. B., Dorwart, M., Naruse, S., Thomas, P. J., and Muallem, S. (2006) Coupling modes and stoichiometry of Cl^-/HCO_3^- exchange by slc26a3 and slc26a6. *J. Gen. Physiol.* **127,** 511–524
53. Coulter-Mackie, M. B., White, C. T., Hurley, R. M., Chew, B. H., and Lange, D. (1993) Primary Hyperoxaluria Type 1, in *GeneReviews* (Pagon, R. A., Bird, T. D., Dolan, C. R., and Stephens, K., eds) Seattle, WA
54. Florin, T., Neale, G., Gibson, G. R., Christl, S. U., and Cummings, J. H. (1991) Metabolism of dietary sulphate. Absorption and excretion in humans. *Gut* **32,** 766–773
55. Kerr, B. J., Weber, T. E., Ziemer, C. J., Spence, C., Cotta, M. A., and Whitehead, T. R. (2011) Effect of dietary inorganic sulfur level on growth performance, fecal composition, and measures of inflammation and sulfate-reducing bacteria in the intestine of growing pigs. *J. Anim. Sci.* **89,** 426–437
56. Ruppin, H., Bar-Meir, S., Soergel, K. H., Wood, C. M., and Schmitt, M. G., Jr. (1980) Absorption of short-chain fatty acids by the colon. *Gastroenterology* **78,** 1500–1507
57. Rossi, A., and Superti-Furga, A. (2001) Mutations in the diastrophic dysplasia sulfate transporter (DTDST) gene (SLC26A2). 22 novel mutations, mutation review, associated skeletal phenotypes, and diagnostic relevance. *Hum. Mutat.* **17,** 159–171